Florida International University

FIU Digital Commons

12-1-2021

A low-complexity FS-MPDPC with extended voltage set for grid-connected converters

Shamini Dharmasena
Florida International University

Temitayo O. Olowu
Florida International University

Arif I. Sarwat
Florida International University

Follow this and additional works at: https://digitalcommons.fiu.edu/all_faculty

IET Energy Systems Integration

天津大学 Tianjin University | IET The Institution of Engineering and Technology | WILEY

ORIGINAL RESEARCH PAPER

A low-complexity FS-MPDPC with extended voltage set for grid-connected converters

Shamini Dharmasena [iD] | Temitayo O. Olowu | Arif I. Sarwat

Department of Electrical and Computer Engineering, Florida International University, Miami, Florida, USA

Correspondence

Shamini Dharmasena, Department of Electrical and Computer Engineering, Florida International University, Miami, Florida, USA.
Email: ikona001@fiu.edu

Abstract

The conventional finite control set model predictive control (FS-MPC) for converter control is a well-studied area, but performance degradation due to the finite candidate vector set is still limiting its practical applications. Extending the voltage vector set using discrete space vector modulation has been proposed as a solution to overcome the limitations, but the brute-force search inherent to FS-MPC increases the computational complexity for a larger voltage set. This paper proposes a technique to alleviate the above issue by avoiding the brute-force search that is being executed in FS-MPC. The technique utilises the basics of *direct-power-control* theory to cut down the number of candidate voltage vectors applied in each cycle in the optimization problem. In this work, a design example having a voltage vector set of 37 elements is considered, and the proposed technique narrows down the search to eight optimal vectors. The proposed controller is specifically designed for active–reactive power control of a grid-connected converter that interlinks an energy storage system to the grid. The system is modelled in MATLAB Simulink environment and simulations are carried out to analyse the performance in all four active–reactive bidirectional power flow modes. Results validate the performance of the controller, both in steady-state and transient conditions. Further, the reduction in computational complexity due to the proposed algorithm is evaluated. It is observed that the number of computations was reduced approximately by 75% after applying the proposed algorithm for a system with a 37 voltage vector set.

1 | INTRODUCTION

Large scale integration of the renewable energy generation in modern power grids is highly desired in order to address the growing energy demand and environmental concerns. However, the increased levels of penetration of distributed energy resources (DERs) (which are mainly from renewable energy) can weaken the rigidity and stability of the grid. Some of the challenges that stem from increased DER penetration are power quality issues, reverse power flow, low inertia, voltage and frequency fluctuations, among others [1]. Battery energy storage systems (BESSs) have proven to be a viable solution for addressing some of the challenges with renewable energy-based DERs. BESSs are capable of operating in very high power ramp rate which is mostly used to reduce high frequency variability when coupled with photovoltaic (PV) systems.

Further, aggregated electric vehicles (EVs) (e.g. EV parks) also have the potential to act as energy storage with bidirectional power transfer capability. With the increased use of EVs, this has become a viable method for current harmonic compensations, active and reactive power transfers. These energy storage systems operates in all the four power quadrants (absorbing and injecting, active and reactive power). Therefore, they can play an important role in the power quality management, autonomous grid forming and maintaining grid stability of distribution networks. These functionalities of classically controlled DERs are achieved through advance power electronics and controls [2].

Grid supporting smart inverter–connected (SI) DERs are being used to maintain grid voltage and frequency within the acceptable range with active and reactive power control (P–Q control) [3]. Unlike conventional power generation techniques,

SI-based DERs are capable of fast dynamic control of the distribution network parameters. For better performance of SI-based DERs, advanced control techniques have become highly imperative.

The conventional control of voltage source converter (VSC) with proportional–integral (PI) control can be disadvantageous in highly dynamic systems with constant perturbations. This is because conventional PIs are pre-tuned to certain system parameters and they might not provide the same expected performance under different dynamic conditions. Also PI controllers are characterised by slow transient response [4]. The direct power control (DPC) technique was introduced as an alternative and it uses a lookup table with predefined switching states [5]. There are various developments of DPC designed to operate in constant switching frequency, including grid voltage modulated–direct power control (GVM-DPC) and sliding-mode direct power control (SM-DPC) [6].

The model predictive control (MPC) for converter control has gained huge popularity in the power electronic research community with the evolution of powerful and fast microprocessors. MPC is a promising control technique for power converters due to its desirable features such as ability to handle multiple inputs/outputs, easily handle system constraints and non-linearities and fast dynamic response [7]. There are two divisions of the MPC used for grid connected converters; model predictive direct power control (MPDPC) [8, 9] and model predictive current control (MPCC) [10, 11]. In MPCC, the grid current is used as the state variable to be controlled. Whereas in MPDPC, the active and reactive power injected and/or absorbed by the converter is controlled. Therefore, MPDPC is well suited for the bidirectional control of grid connected converters.

Among two major variants of the MPC which are finite control set model predictive control (FS-MPC) and continuous control set model predictive control (CCS-MPC), FS-MPC is the most commonly used technique for power converters [12]. The reason is that, the converter systems have well known mathematical models and can easily identify the finite number of switching states as the finite control set. FS-MPC uses the mathematical model of the converter to predict the behaviour of the state variables at each sampling period for all the control inputs in the finite control set.

In conventional FS-MPC, the optimal candidate from the finite control set is chosen by performing a brute-force search. This can exhaust the processes, especially if the control set is large, as it could involve a huge number of computations. Therefore, research has been carried out to develop techniques to reduce the computational complexity involved in FS-MPC with a bigger voltage set. The state-of-the-art of the research on this regard is extensively analysed in Section 2.

In this paper a complexity reduction technique to avoid the brute-force search in FS-MPDPC is proposed and hereinafter it will be referred as low complexity–FS-MPDPC (LC-FS-MPDPC). The LC–FS-MPDPC is designed for a grid connected converter to control the bidirectional active–reactive power flow. The comparative advantages of this controller compared to the state-of-the-art and the novelty of this work is presented in the later part of Section 2.

This paper is structured into seven sections. Section 2 presents the state-of-the-art and motivation for the work and Section 3 provides a brief introduction to the system considered for the study. Then, in Section 4 the application of conventional FS-MPDPC for the system is presented and in Section 5 the LC–FS-MPDPC is presented. In order validate the effectiveness of the LC–FS-MPDPC, Section 6 provides the simulation results together with a comparison of the computational complexities and performances. Section 7 concludes the paper.

2 | MOTIVATION AND THE STATE-OF-THE-ART

In FS-MPC, the voltage chosen as the optimal vector is applied to the whole control cycle. For a three-phase two-level converter, the operable voltage vector set without employing any modulation technique is limited to seven. The size of the converter voltage vector set is one of the major disadvantages of FS-MPC for three-phase power applications, which causes power ripples and current harmonics. For multi-phase systems, this issue is not very critical since the finite voltage vector set is larger and can emulate a more continuous behaviour [13, 14]. Although employing a higher switching frequency for conventional FS-MPC alleviates this issue, it can increase switching losses.

To circumvent this limitation, the discrete space vector modulation–based (DSVM) FS-MPC techniques have been proposed in the literature. This generates a bigger vector set for optimization [15, 16]. DSVM–FS-MPC applies multiple voltage vectors in a single switch cycle, thus creating a virtual vector space which can effectively suppress the harmonic content in current waveforms. But again, when the vector set gets bigger, the brute-force search of FS-MPC becomes computationally expensive. Variable switching frequency is another complication that comes with virtual vector synthesis [17]. There are other constrains as well, such as maintaining a minimum switching frequency to reduce losses and reducing the common mode voltage. In the light of the above concerns, different techniques have been developed and proposed in the literature to address these issues [18].

Several significant approaches that have been proposed in the literature to reduce the computational complexity are comprehensively discussed here with their respective references. First one is the deadbeat technique, in which the desired converter voltage vector for the next state is calculated based on line current predictions [10, 19, 20]. Then, the calculated desired voltage is used as a reference to narrow down the search area in the vector space, which reduces the number of candidate vectors. Since the desired voltage is calculated using the system model equations, the deadbeat technique–based MPC is heavily dependent on system parameters. Hence, the deadbeat technique is not robust for system perturbations and requires a higher sampling frequency to achieve better

performance. This method also involves an additional computational load for reference voltage calculations in each cycle. The paper [19] proposes a deadbeat DSVM–FS-MPC for a grid connected VSC. The converter reference voltage is calculated, and its magnitude and phase angle is used to reduce the search area in the vector space. This technique highly reduces the number of voltage vectors used for optimization, but still the drawbacks mentioned earlier persist.

The authors of [21] have proposed the extended model predictive-sliding mode control (EMP-SMC) technique for grid connected converters. They have applied sliding-mode theory for d–q axis currents which is used as the basis to narrow down the search area in the vector space. A pre-calculated lookup table is used to select the candidate vectors for the optimization at each case identified by the sliding mode theory. In this paper, a vector set of 19 is considered and the proposed method has reduced the number of candidates to 10 for optimization. In this method, the lookup table formulation consumes considerable computation power and the complexity of formulation increases as the size of the vector set increases. A bigger vector set increases the size of the look table as well. Therefore, EMP-SMC can be almost impractical when the size of the vector set increases.

The modified FS-MPC proposed in [22] uses a technique that has a pre-selection stage and two optimization stages for voltage vector selection process in the vector space to reduce computations in DSVM–FS-MPC. Initially, a pre-selection process is executed to reduce the size of the vector set to half. In the first optimization stage, only the real vectors in the pre-selected region is considered for the optimization. Then the virtual vectors closest to the optimal real vector produced in the first stage is selected for the second stage optimization. This technique cuts down unnecessary voltage vectors for optimization. But the complicated process with several optimization stages in each switching cycle makes the technique computationally expensive.

Another technique proposed in the literature to improve the performance of conventional FS-MPC is duty cycle control method [23, 24]. Rather than extending the voltage set, the duty cycles of the real vectors are controlled to obtain the optimal vector. In [25], the duty cycle control is applied for a double vector optimization scheme. Here, the first optimum voltage is calculated similar to conventional FS-MPC and then the second vector is selected close to the first one to reduce the number of switching. The duty cycles of two vectors were then calculated minimising the cost function. One of the key contributions by this paper is that it avoids the use of zero voltage vectors in order to reduce common-mode voltage. Although this method has a lower computational complexity and reduced common mode voltage, the current harmonic distortion is higher compared to other techniques discussed earlier. Also, the duty cycle control technique is highly disadvantaged due to inherent variable switching frequency. An improved dual-vector–based predictive duty cycle control strategy is proposed in the paper [26], which states that it eliminates the time consuming procedure of duty-cycle optimization. The proposed controller in [26] utilises the cost function for both best

vector selection and duration derivation. Another duty cycle control based MPC is proposed in [27], and this strategy determines the mapping between variables by exploring the dual relationship of vector synthesis and duty cycles.

In contrast to the above discussed literature, the key contributions proposed in this paper can be highlighted as follows:

1. *Constant switching frequency.*: The proposed technique has a constant switching frequency ($3f_s$) for space vector generation.
2. *Bidirectional power control and consideration of grid constraints in objective function.*: Almost all the publications discussed previously (and others) focussed on unidirectional power flow (either rectifier or inverter operation). The proposed technique is designed and validated for bidirectional active and reactive power control. And there are many practical operational constraints affecting the controller operation of a grid connected converter. But none of the works discussed earlier contemplate these constraints and this paper incorporates the operational constrains into the objective function.
3. *Improved computational efficiency.*: Unlike other methods in literature, the proposed approach is formulated based on MPDPC. Hence the control problem is in the stationary reference frame avoiding additional steps needed to compute the park transformation. In addition to the contributions mentioned above, a computational complexity comparison of the proposed technique is presented in Section 6.3.

3 | GRID-CONNECTED BESS AS A CASE STUDY

The grid network used for the study is illustrated in Figure 1. An energy storage system is connected to the distribution grid through a three-phase two-level VSC. Also, the system is equipped with a simple inductor (L) filter and a resistor for passive damping. The controller generates necessary gate control signals for the converter.

As stipulated in the IEEE 1547–2018 standard [28], grid-connected DERs' SIs should be capable of providing grid supporting ancillary services such as P–Q control for voltage and frequency regulation. Therefore, converters that interlink energy storage systems to the grid should be able to operate in all the four quadrants of the P–Q power flow and smoothly transit between these operation modes seamlessly.

There are two basic functionalities expected from the controller. First, the converter should inject or absorb active and reactive power to/from the grid according to the grid requirements and dynamics. Second, the controller should maintain the permissible charge limits of the energy storage by feeding active power to the energy storage. Therefore, the instantaneous reference power (P_{ref} and Q_{ref}) is fed to the controller based on the magnitude of grid voltage, frequency fluctuations, smart inverter settings and the charge state of energy storage. The sign convention used in this paper as the
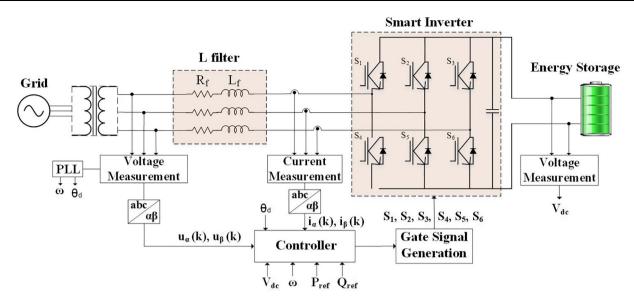
FIGURE 1 The system used for the study: the energy storage connected to the grid via a three-phase two-level voltage source converter and an L filter

power flow from energy storage to the grid is positive and negative otherwise. The power flow is constrained by the maximum apparent power of the converter, S_r.

4 | CONVENTIONAL FS-MPDPC FOR a GRID-CONNECTED CONVERTER

MPC is a model based control strategy and the system under study can be simply modelled by (1). Here, u_{abc}, e_{abc}, i_{abc} are three-phase grid-end voltages, converter-end voltages and grid currents, respectively. R_f and L_f are the filter damping resistance and the filter inductance.

$$e_{abc} = R_f i_{abc} + L_f \frac{di_{abc}}{dt} + u_{abc} \tag{1}$$

The time-varying nature of sinusoidal voltage–current components complicates the implementation of the control algorithm. To reduce this complexity, the voltage and current measurements are converted into a stationary reference frame using Clarke transformation (*abc to* $\alpha - \beta$). The $\alpha - \beta$ transformed system model can be expressed as shown in Equation (2).

$$e_{\alpha\beta} = R_f i_{\alpha\beta} + L_f \frac{di_{\alpha\beta}}{dt} + u_{\alpha\beta} \tag{2}$$

To apply FS-MPC, the system equations are converted to discrete time domain using forward Euler transformation. The discrete state space representation of the system [29] is given in Equation (3)

$$X(k+1) = AX(k) + BU(k) + M \tag{3}$$

where,

$$X = [i_\alpha, i_\beta]^T, U = [e_\alpha, e_\beta]^T, A = \begin{bmatrix} \left(1 - \frac{T_s R_f}{L_f}\right) & 0 \\ 0 & \left(1 - \frac{T_s R_f}{L_f}\right) \end{bmatrix}$$

$$B = \begin{bmatrix} \frac{T_s}{L_f} & \frac{T_s}{L_f} \end{bmatrix}, M = \begin{bmatrix} \frac{-T_s u_\alpha}{L_f} & \frac{-T_s u_\beta}{L_f} \end{bmatrix}, T_s$$

is the sampling time.

According to instantaneous power theory, active and reactive power at the point of common coupling (PCC) is $P = \frac{3}{2}(u_\alpha i_\alpha + u_\beta i_\beta)$ and $Q = \frac{3}{2}(u_\beta i_\alpha - u_\alpha i_\beta)$, respectively. The grid voltages can be approximated as $u_\alpha(k + 1) = u_\alpha(k)$, $u_\beta(k + 1) = u_\beta(k)$, since the sampling frequency is relatively much higher when compared to the grid frequency. Therefore, the active and reactive power for the next state can be simplified as expressed in Equation (4).

$$\begin{aligned} P(k+1) &= 1.5(u_\alpha(k)i_\alpha(k+1) + u_\beta(k)i_\beta(k+1)) \\ Q(k+1) &= 1.5(u_\beta(k)i_\alpha(k+1) - u_\alpha(k)i_\beta(k+1)) \end{aligned} \tag{4}$$

Then, by substituting Equation (3) into Equation (4), the predictive model for the system is derived and is as expressed in Equation (5). In this model, the prediction horizon is extended to two in order to compensate the delay in the actual digital control.

$$\begin{bmatrix} P(k+2) \\ Q(k+2) \end{bmatrix} = \begin{bmatrix} \left(1 - \frac{T_s R_f}{L_f}\right) & -T_s\omega \\ T_s\omega & \left(1 - \frac{T_s R_f}{L_f}\right) \end{bmatrix} \begin{bmatrix} P(k+1) \\ Q(k+1) \end{bmatrix} \\ + \frac{3T_s}{2L_f} \begin{bmatrix} |\vec{u}_{\alpha\beta}|^2 - \text{Re}(\vec{u}_{\alpha\beta}\vec{e}_{\alpha\beta}^*) \\ -\text{Im}(\vec{u}_{\alpha\beta}\vec{e}_{\alpha\beta}^*) \end{bmatrix} \tag{5}$$

In FS-MPDPC a finite set of converter voltage vectors are considered to predict the next state power using the Equation (5). Without any modulation technique in use, the converter AC side voltages correspond to the possible switching states which is eight in number for a three-phase two-level converter. The eight switch states generate seven unique voltage vectors as given in Equation (6), in which n is the switching state and V_{DC} is the DC link voltage.

$$e_n = \begin{cases} \frac{2}{3} V_{dc} e^{jn\frac{\pi}{3}} & n = 1, 2, \ldots, 6 \\ 0 & n = 0, 7 \end{cases} \quad (6)$$

4.1 | Objective function and optimization

The active power reference (P_{ref}) and reactive power reference (Q_{ref}) values are provided to the control system as mentioned in Section 3. The objective function given in Equation (7) consists of two conditions and a constraint. The two conditions are designed with a quadratic norm to minimise the power error. λ_1 and λ_2 are the weights of each component in the objective function. The maximum apparent power limitation of the converter is applied as a constraint.

$$Min : \{ J(k + 2) = \lambda_1 (P(k + 2) - P_{ref})^2 \\ + \lambda_2 (Q(k + 2) - Q_{ref})^2 \}$$

$$Subjected \ \ to : P(k + 2)^2 + Q(k + 2)^2 < S_r^2 \quad (7)$$

The objective function is solved for all the predicted power values that correspond to the candidate voltage vectors of the converter. Then the voltage vector that generates the minimum cost is selected as the input for the next state operation.

5 | VIRTUAL VECTOR SYNTHESIS AND PROPOSED ALGORITHM

As discussed extensively in Section 2, the use of a finite voltage set as the control input in FS-MPC can degrade performance, leading to a more discrete and variable output with a lot of ripples in the current and power waveforms. A near-continuous flow can be obtained by increasing the number of elements in the voltage set. Therefore, to address this issue an extended voltage vector set can be used with virtual vector synthesis. This concept was proposed in [22] which uses 37 distinct voltage vectors that are uniformly distributed in the vector space. In this paper, the converter voltage vector space (CVVS) is divided into three concentric hexagons on which 37 voltage vectors are placed equidistantly. Among them 7 are the real switch voltages of a three phase two level converter and

the rest are virtual voltages. The same vector distribution in the CVVS is considered in this paper and it is given in Figure 2a in which green square markers indicate the real switch states. Virtual vectors (VV) are synthesised using the DSVM technique in which VVs are formulated as vector summations of real voltages. The three elements of a switch state represent the turn-on ratio of the switches of the three phases. For example,

$$Z \, Z \, 0 \; \Rightarrow \; ZT_s * V_1 + ZT_s * V_3 + 0T_s * V_5 + ZT_s * V_7$$
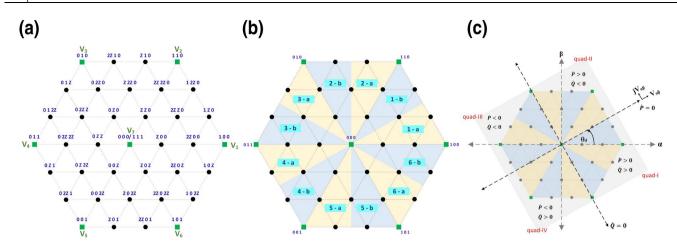$$0 \, 2Z \, Z \; \Rightarrow \; 0T_s * V_1 + 2ZT_s * V_3 + ZT_s * V_5 + 0T_s * V_7$$

Here, the VV related to ZZ0 switch state is composed by applying V_1, V_3 and V_7 voltages for time periods of ZT_s each. The turned-on time of phase C switch is zero for this case, and V_7 is the zero vector. The variable $Z = 1/3$ and T_s is the sampling period. The significance of the selected set is that the VV generation doesn't lead to a variable frequency switching and it increases to $3f_s$. The switching states and their relevant voltage vectors used in this analysis are given in the Table.1.

5.1 | Proposed LC–FS-MPDPC to constrict the optimal vector search

As mentioned earlier, a total of 37 voltage vectors are used as the finite vector set to solve the optimization problem. To reduce the number of computations required in each switch cycle, a simplification strategy for the vector search is proposed in this section.

The basis of DPC theory is utilised here to reduce the complexity involved in virtual vector integrated FS-MPDPC. The instantaneous active and reactive powers are the final deliverable that needs to be regulated, by the grid connected converter for this case, and they are analogous to the role of the torque and flux amplitude in direct torque control (DTC) of the induction motor. Inspired by DTC applied to the induction motor in [30], an algorithm is developed to reduce the vector selection area from the virtual vector space. In conventional DPC, offline switching tables are used to determine the inverter voltage vector to be applied based on the desired active and reactive power variations and the information of the grid voltage at PCC [31]. As stated by the DPC theory, each switching voltage vector of the converter in the CVVS has a different influence on the change of instantaneous active–reactive powers and this influence varies with the angular position of the changing grid voltage, $V_{\alpha\beta}$ [32, 33]. Therefore, optimal switching functions can be applied systematically based on power injection/absorption requirements under different angular positions of $V_{\alpha\beta}$.

In this paper the DPC concept is incorporated in developing the algorithm to simplify the vector search. As presented in [33], two perpendicular planes are defined on the CVVS which are aligned along the grid voltage vector, $V_{\alpha\beta}$ and $jV_{\alpha\beta}$. Hereinafter we refer to these planes as grid

FIGURE 2 (a) Locus of the considered real and virtual switching vectors in CVVS, (b) Division of the CVVS into 12 sectors (1-a, 1-b, …), (c) Approximated behaviour of $\dot{P}$ and $\dot{Q}$ in the GVVS

T A B L E 1 Converter voltage vectors

Switching state			Voltage	Switching state			Voltage	Switching state			Voltage	Switching state			Voltage
0/1	0/1	0/1	0	Z	2Z	0	$\frac{2}{3\sqrt{3}}V_{dc}e^{\frac{\pi}{2}j}$	0	2Z	2Z	$\frac{4}{9}V_{dc}e^{\pi j}$	2Z	0	1	$\frac{2\sqrt{7}}{9}V_{dc}e^{\frac{-4\pi}{9}j}$
Z	0	0	$\frac{2}{9}V_{dc}e^{0j}$	Z	1	0	$\frac{2\sqrt{7}}{9}V_{dc}e^{\frac{4\pi}{9}j}$	0	1	1	$\frac{2}{3}V_{dc}e^{\pi j}$	Z	0	Z	$\frac{2}{9}V_{dc}e^{\frac{-\pi}{3}j}$
2Z	0	0	$\frac{4}{9}V_{dc}e^{0j}$	2Z	1	0	$\frac{2\sqrt{7}}{9}V_{dc}e^{\frac{5\pi}{6}j}$	0	Z	2Z	$\frac{2}{3\sqrt{3}}V_{dc}e^{\frac{-5\pi}{6}j}$	2Z	0	2Z	$\frac{4}{9}V_{dc}e^{\frac{-\pi}{3}j}$
1	0	0	$\frac{2}{3}V_{dc}e^{0j}$	0	Z	0	$\frac{2}{9}V_{dc}e^{\frac{2\pi}{3}j}$	0	Z	1	$\frac{2\sqrt{7}}{9}V_{dc}e^{\frac{-8\pi}{9}j}$	1	0	1	$\frac{2}{3}V_{dc}e^{\frac{-\pi}{3}j}$
2Z	Z	0	$\frac{2}{3\sqrt{3}}V_{dc}e^{\frac{\pi}{6}j}$	0	2Z	0	$\frac{4}{9}V_{dc}e^{\frac{2\pi}{3}j}$	0	2Z	1	$\frac{2\sqrt{7}}{9}V_{dc}e^{\frac{-7\pi}{9}j}$	2Z	0	Z	$\frac{2}{3\sqrt{3}}V_{dc}e^{\frac{-\pi}{6}j}$
1	Z	0	$\frac{2\sqrt{7}}{9}V_{dc}e^{\frac{\pi}{9}j}$	0	1	0	$\frac{2}{3}V_{dc}e^{\frac{2\pi}{3}j}$	0	0	Z	$\frac{2}{9}V_{dc}e^{\frac{-2\pi}{3}j}$	1	0	2Z	$\frac{2\sqrt{7}}{9}V_{dc}e^{\frac{-2\pi}{9}j}$
1	2Z	0	$\frac{2\sqrt{7}}{9}V_{dc}e^{\frac{2\pi}{9}j}$	0	2Z	Z	$\frac{2}{3\sqrt{3}}V_{dc}e^{\frac{5\pi}{6}j}$	0	0	2Z	$\frac{4}{9}V_{dc}e^{\frac{-2\pi}{3}j}$	1	0	Z	$\frac{2\sqrt{7}}{9}V_{dc}e^{\frac{-\pi}{9}j}$
Z	Z	0	$\frac{2}{9}V_{dc}e^{\frac{\pi}{3}j}$	0	1	Z	$\frac{2\sqrt{7}}{9}V_{dc}e^{\frac{7\pi}{9}j}$	0	0	1	$\frac{2}{3}V_{dc}e^{\frac{-2\pi}{3}j}$				
2Z	2Z	0	$\frac{4}{9}V_{dc}e^{\frac{\pi}{3}j}$	0	1	2Z	$\frac{2\sqrt{7}}{9}V_{dc}e^{\frac{8\pi}{9}j}$	Z	0	2Z	$\frac{2}{3\sqrt{3}}V_{dc}e^{\frac{-3\pi}{2}j}$				
1	1	0	$\frac{2}{3}V_{dc}e^{\frac{\pi}{3}j}$	0	Z	Z	$\frac{2}{9}V_{dc}e^{\pi j}$	Z	0	1	$\frac{2\sqrt{7}}{9}V_{dc}e^{\frac{-5\pi}{9}j}$				

voltage vector space (GVVS). The GVVS is shifted from $\alpha - \beta$ plane by the angular position θ_d which rotates in a synchronous speed. The approximated behaviour of the instantaneous active power first derivative, $\dot{P}$, and the instantaneous reactive power first derivative, $\dot{Q}$, with respect to the planes are as given in the Figure 2c [34]. Therefore, the converter voltage vectors in each quadrant of the GVVS steer the active and reactive power in different directions as illustrated in the Figure 2c. At some positions of θ_d, there are at most three real voltage vectors that provide the same behaviour of $\dot{P}$ and $\dot{Q}$. In this paper a single real vector for each quadrant is selected following the modified Eloy–Garcia approach which provides a better tracking of both P and Q towards their references [34].

The developed controller algorithm can be explained in three steps. The first step is obtaining the relevant real converter voltage vector based on the position of $V_{\alpha\beta}$ in CVVS and the quadrant of operation in GVVS. In order to determine the quadrant of operation in the GVVS, $\dot{P}$ and $\dot{Q}$ are calculated as expressed in Equation (8).

$$\dot{P} > 0 \rightarrow P(k) < P_{ref}, \quad \dot{P} < 0 \rightarrow P(k) > P_{ref}$$
$$\dot{Q} > 0 \rightarrow Q(k) < Q_{ref}, \quad \dot{Q} < 0 \rightarrow Q(k) > Q_{ref} \tag{8}$$

As the GVVS rotates at a synchronous speed, it is necessary to locate the quadrants in the converter vector space at each control cycle to determine the candidate voltage vector set. Therefore, the converter vector space is divided into 12 sectors, which combines the six main sectors each divided into two as shown in Figure 2b and the position of $V_{\alpha\beta}$ is determined with respect to the sectors. Then, based on the sector of $V_{\alpha\beta}$ and the quadrant of operation in GVVS, the suitable real converter voltage vector is selected using Table 2. For example, if V_d is at sector 1-b and both $\dot{P}$ and $\dot{Q}$ needs to be negative, the real voltage vector for converter is chosen as the voltage of '011' switch state which is $\frac{2}{3}V_{dc}e^{\pi j}$.

Then the candidate vector set connected to the obtained real voltage vector needs to be identified. Each real vector is neighboured by six virtual voltage vectors. The real vector, the

six neighbouring virtual vectors and the zero vector are chosen as the candidate vector set to solve the optimization problem. The selection of the vector set is illustrated in Figure 3 which circles-out the vector set related to '110' switch state. In this way the size of the candidate vector set is reduced from 37 to 8 for the optimization.
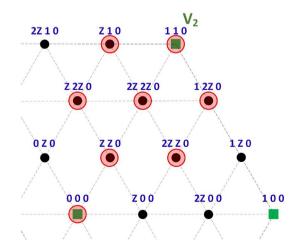
Finally, the process follows the conventional FS-MPDPC technique explained in Section 4 for the constricted candidate voltage vector set. The optimal voltage vector that minimises the objective function is selected for the next state operation and duty ratios are calculated for that. The control algorithm is explicitly illustrated in a block diagram given in Figure 4.

6 | RESULTS AND DISCUSSION

To analyse and validate the performance of the proposed control algorithm, the system is modelled in MATLAB/Simulink. The system parameters used for modelling are given in Table 3. The system is designed with an L filter only to highlight the performance comparisons of different controllers.

6.1 | Steady-state performance analysis

Simulations were carried out under steady state conditions to compare the performance of the conventional FS-MPDPC, FS-MPDPC with extended voltage set and LC–FS-MPDPC with extended voltage set. Figure 5 shows the grid voltage, line current and FFT analysis of line current for each method. It can be clearly observed that the conventional FS-MPDPC with the seven element vector set has a higher harmonic content compared to the other two methods with extended voltage sets. The total harmonic distortion (THD) in line current has a striking reduction from 10.75% in conventional FS-MPDPC to 4.02% in FS-MPDPC with the extended voltage set (especially in the fifth and seventh harmonics). However, the quality of line current has slightly reduced from Figure 5b to Figure 5c. But this slight increase in THD in the LC–FS-MPDPC is almost insignificant when considering the computational simplification achieved. Therefore, unlike the conventional FS-MPDPC, the proposed technique guarantees a better performance with a lower harmonic content.

To further analyse, in Figure 6, the line current in the stationary reference frame ($I_{\alpha\beta}$) is plotted for steady-state conditions to highlight the performance improvement

TABLE 2 Optimal switching table for converter when grid voltage vector at sector k

	$\dot{P}$	$\dot{Q}$	Converter voltage vector @ sector k-a	Converter voltage vector @ sector k-b
Quad-I	>0	>0	e_k	e_k
Quad-II	>0	<0	e_{k+1}	e_{k+1}
Quad-III	<0	>0	e_{k-2}	e_{k-1}
Quad-IV	<0	<0	e_{k+2}	e_{k+3}

FIGURE 3 Selection of the candidate voltage vector set: the vector set connected to V_2 real vector
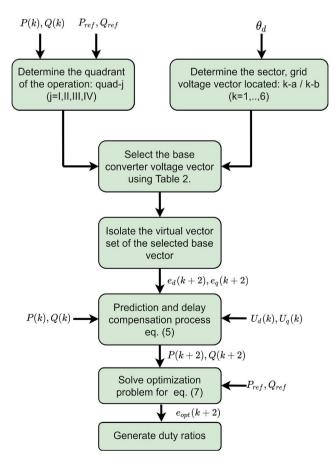

FIGURE 4 Block diagram of controller operation

achieved by introducing virtual vectors to the candidate voltage set. Figure 6a shows the $I_{\alpha\beta}$ plot for the conventional FS-MPC while Figure 6b shows the $I_{\alpha\beta}$ plot using the proposed controller. It can be seen that the line currents perform better with the proposed controller.

A comparison of active and reactive power ripples for both conventional FS-MPDPC and LC–FS-MPDPC is simulated and shown in Figure 7. The standard deviation function is applied to calculate the active and reactive power ripples at two different reference points. The active and reactive power rip-

ples are calculated under the two scenarios of $P_{ref} = 4000\ W$, $Q_{ref} = 3000\ var$ and $P_{ref} = 2000\ W$, $Q_{ref} = 1000\ var$. A quantitative analysis of ripple percentages are illustrated in Figure 8. The ripple percentages are significantly low for LC–FS-MPDPC compared to the conventional FS-MPDPC in all the scenarios. Also, from the figure it is evident that the percentage ripple reduction is higher at the light power reference point ($P_{ref} = 2000\ W$, $Q_{ref} = 1000\ var$). This validates that VV implementation improves the power performance by a wider range.

6.2 | Transient performance analysis

To further validate the performance of the LC–FS-MPDPC, simulations are carried out for several transient situations. In the first case, P_{ref} and Q_{ref} are varied so that the active power and reactive power vary linearly with time. Four scenarios were simulated to demonstrate the operation in all four quadrants of the GVVS. The controller tracks the linear variations of the power references perfectly as depicted in Figure 9. The figure provides the performance in all four quadrants, quad-I: $\dot{P} > 0$, $\dot{Q} > 0$, quad-II: $\dot{P} > 0$, $\dot{Q} < 0$, quad-III: $\dot{P} < 0$, $\dot{Q} < 0$ and quad-IV: $\dot{P} < 0$, $\dot{Q} > 0$ in Figure 9a–d, respectively. The line current behaviour is also shown for each condition.
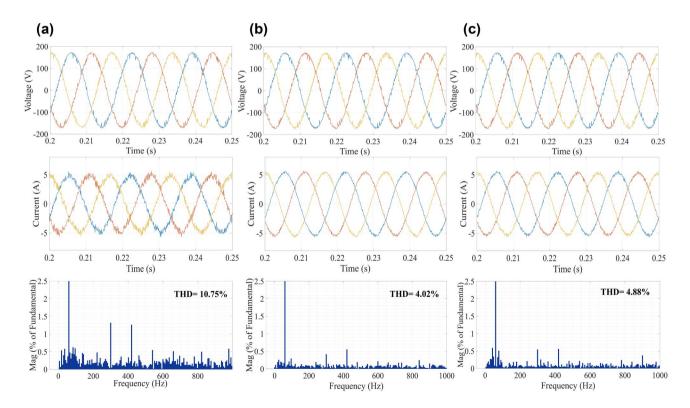
TABLE 3 Parameters used for simulations

Parameters	Values
Converter rated power (S_r)	7.5 kVA
DC link voltage (V_{dc})	500 V
Filter resistance (R_f)	0.2 Ω
Filter inductance (L_f)	15 mH
Sampling frequency (F_s)	10 kHz
Fundamental frequency	60 Hz
Grid voltage	120 V
Weights λ_1, λ_2	1, 1

FIGURE 5 Steady state performance of grid voltage, line current and FFT analysis of line current for (a) conventional FS-MPDPC, (b) FS-MPDPC with extended voltage set, and (c) LC–FS-MPDPC with extended voltage set
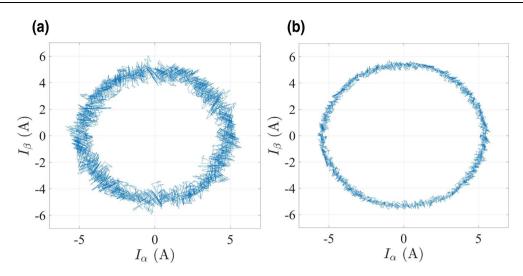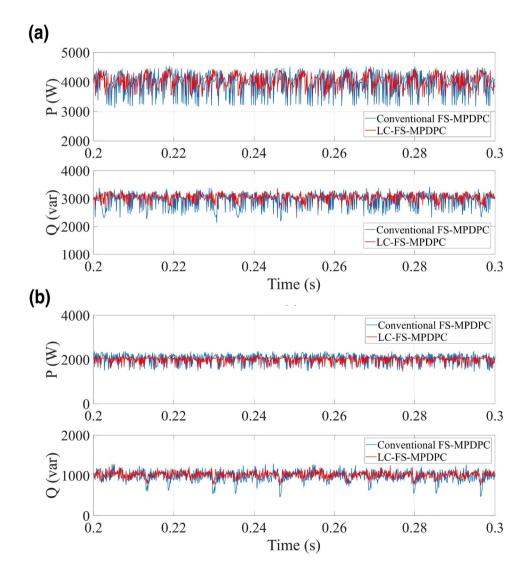
FIGURE 6 Plot of $I_{\alpha\beta}$ at steady-state for (a) conventional FS-MPDPC, (b) LC–FS-MPDPC with extended voltage set

FIGURE 7 Active power and reactive power wave forms for conventional FS-MPDPC and LC–FS-MPDPC with extended voltage set at (a) $P_{ref} = 4000\ W$, $Q_{ref} = 3000\ var$, (b) $P_{ref} = 2000\ W$, $Q_{ref} = 1000\ var$

The second transient simulation was to test the capability of controlling bidirectional power flow. A grid connected converter operates in four power flow modes; capacitive-power source ($P > 0$, $Q > 0$), capacitive-load ($P < 0$, $Q > 0$), inductive-power source ($P > 0$, $Q < 0$) and inductive-load ($P < 0$, $Q < 0$). Active power and reactive power commands were varied to test the transition performance between the two power modes. In Figure 10, a smooth transition between capacitive-power and capacitive-load modes can be observed and the transition time is around 0.8 mS for both active and reactive power. A fast and accurate convergence to the commanded power values are observed for inductive-power source and inductive-load modes as well which is shown in Figure 11. After the transien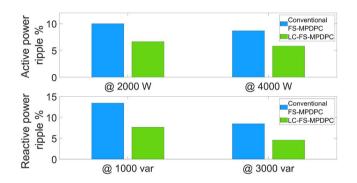t condition, a good steady-state operation is observed in all the four power modes and the ripples in both active power and reactive power are within the acceptable range.

6.3 | Computational complexity comparisons

One of the main objectives of this paper is to propose a technique that reduces the hardware execution time by simplifying the optimal vector search of the controller. FS-MPDPC has several processing steps which include, P–Q predictions, delay compensations and optimization of the objective function. Each of this step involves a certain number
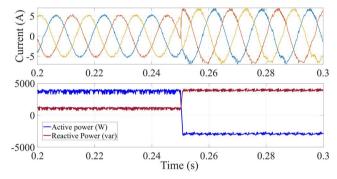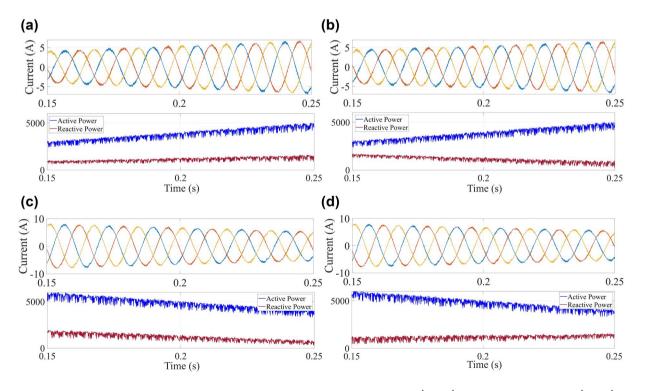

FIGURE 8 Comparisons of the active and reactive power ripples for conventional FS-MPDPC and LC–FS-MPDPC with extended voltage set

FIGURE 10 Transient performance: transition between capacitive-power source and capacitive-load modes

FIGURE 9 Transient performance: grid current, active power and reactive power for (a) quad-I ($\dot{P} > 0$, $\dot{Q} > 0$) operation, (b) quad-II ($\dot{P} > 0$, $\dot{Q} < 0$) operation, (c) quad-III ($\dot{P} < 0$, $\dot{Q} < 0$) operation, (d) quad-IV ($\dot{P} < 0$, $\dot{Q} > 0$) operation

of computations which include multiplications and additions. When quantifying the number of computations, it directly depends on the number of candidate voltage vectors. The number of computations involved in these steps for conventional FS-MPDPC, FS-MPDPC with extended voltage set and
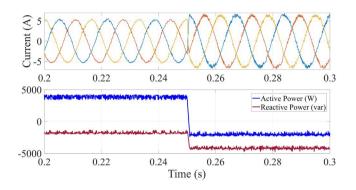

FIGURE 11 Transient performance: transition between inductive-power source and inductive-load modes

TABLE 4 A comparison on number of computations

Technique	Number of additions	Number of multiplications	Total computations
Conventional FS-MPDPC	101	118	219
FS-MPDPC with extended voltage set	491	538	1029
LC–FS-MPDPC with extended voltage set	118	139	257

TABLE 5 A comparison on timing performance

Technique	Execution time (μs)
Conventional FS-MPDPC	30
FS-MPDPC with extended voltage set	68
LC–FS-MPDPC with extended voltage set	36

TABLE 6 Comparison between the existing and proposed schemes

	Deadbeat FS-MPC [19]	EMP-SMC [21]	Two-stage optimization [22]	Duty-cycle control [25]	LC-FS-MPDPC
Park transformation	Not required	Required	Required	Not required	Not required
PLL	Not required	Required	Required	Not required	Required
Switching frequency	Constant	Constant	Constant	Variable	Constant
Robustness for parameter variations	Low	High	High	High	High

LC–FS-MPDPC with extended voltage set are quantified and shown in Table 4. Other than the aforementioned processing steps, the proposed technique involves additional computations for the constriction algorithm which are added to the total computations given in Table 4.

A striking reduction in computations can be observed due to the constriction algorithm, which is almost a reduction of 70%. The computations are a little high in the LC–FS-MPDPC compared to the conventional FS-MPDPC method. However, when considered in terms of improvement in performance attained due to virtual vectors which is indicated in Figure 5, this increment in computations can be deemed negligible.

The execution time of an algorithm is another measure of efficiency, but it depends on implementation details such as hardware and software configuration, parallel processors etc. of the computer. Since this is a comparison between three algorithms, simulations are done in the same processor platform under similar conditions to avoid the dependence on the platform. Therefore, the minimum execution time out of 100 executions has been reported here as it provides the closest approximate execution time for the algorithm with minimal overhead time. The timing performance of the proposed algorithm and the conventional schemes are given in Table 5.

Four state-of-the-art techniques to reduce the computational complexity that were discussed in the Section 2 are comparatively analysed in Table 6. One publication from each of the technique is considered here. It is quite difficult to execute a comprehensive performance comparison between the considered publications because their results were generated under dissimilar conditions and settings. Therefore, a general comparison based on certain features are considered for the evaluation.

7 | CONCLUSION

This paper proposes a complexity reduction technique to minimise the computational load involved in FS-MPDPC with an extended voltage vector set. The controller is designed for bidirectional active–reactive power flow control of a converter that interlinks a BESS with the grid. The developed control algorithm is inspired by the DPC theory, in which

predetermined switching combinations are used for power flow control based on the desired active and reactive power variations and the instantaneous angular position of the grid voltage. This constriction algorithm reduced the size of the candidate voltage vector set for optimization from 37 to 8. The effectiveness of the controller is evaluated both under steady-state and transient conditions. The harmonic analysis of line current at steady-state exhibits a significant improvement in the LC–FS-MPDPC compared to the conventional FS-MPDPC in which the THD has reduced from 10.75% to 4.88%. Further, the number of addition and multiplication operations is considerably reduced from 1029 in FS-MPDPC with the extended voltage set to 257 after applying the proposed technique. The controller performance in all power flow modes is analysed and smooth transitions between different power modes are observed. The system is also analysed for operation in all four quadrants of the GVVS. The obtained results verify that the LC–FS-MPDPC provides almost a similar performance to FS-MPDPC for an extended voltage set, but requires lesser computations.

ACKNOWLEDGEMENT

ORCID

Shamini Dharmasena https://orcid.org/0000-0002-0663-8166

REFERENCES

1. Olowu, T., et al.: Future challenges and mitigation methods for high photovoltaic penetration: a survey. Energies. 11(7), 1782 (2018)
2. Moghaddami, M., Sarwat, A.I.: Single-phase soft-switched AC-AC matrix converter with power controller for bidirectional inductive power transfer systems. IEEE Trans. Ind. Appl. 54(4), 3760–3770 (July 2018)
3. Moghadasi, A., et al.: Active and reactive power control method for three-phase PV module-integrated converter based on a single-stage inverter. In: 2017 IEEE Applied Power Electronics Conference and Exposition (APEC), pp. 1357–1362 (2017)
4. Wickramasinghe Abeywardana, D.B., et al.: Single-phase boost inverter-based electric vehicle charger with integrated vehicle to grid reactive power compensation. IEEE Trans. Power Electron. 33(4), 3462–3471 (Apr 2018)
5. Gui, Y., et al.: Voltage-modulated direct power control for a weak grid-connected voltage source inverters. IEEE Trans. Power Electron. 34(11), 11 383–11 395 (Nov 2019)
6. Gui, Y., et al.: Sliding mode control with grid voltage modulated DPC for voltage source inverters under distorted grid voltage. CPSS Trans. Power Electron. Appl. 4(3), 244–254 (Sep 2019)
7. Vazquez, S., et al.: Model predictive control: a review of its applications in power electronics. EEE Ind. Electron. Mag. 8(1), 16–31 (2014)
8. Hu, J., Zhu, J., Dorrell, D.G.: Model predictive control of grid-connected inverters for pv systems with flexible power regulation and switching frequency reduction. IEEE Trans. Ind. Appl. 51(1), 587–594 (2015)
9. Zhang, Y., Qu, C.: Model predictive direct power control of pwm rectifiers under unbalanced network conditions. IEEE Trans. Ind. Electron. 62(7), 4011–4022 (2015)
10. Parvez Akter, M., et al.: Modified model predictive control of a bidirectional AC-DC converter based on Lyapunov function for energy storage systems. IEEE Trans. Ind. Electron. 63(2), 704–715 (Feb 2016)
11. Moghadasi, A., et al.: A model predictive power control approach for a three-phase single-stage grid-tied PV module-integrated converter. IEEE Trans. Ind. Appl. 54(2), 1823–1831 (Mar 2018)
12. Panten, N., Hoffmann, N., Fuchs, F.W.: Finite control set model predictive current control for grid-connected voltage-source converters with LCL filters: a study based on different state feedbacks. IEEE Trans. Power Electron. 31(7), 5189–5200 (2016)
13. Dharmasena, S., Choi, S.: Model predictive control of five-phase permanent magnet assisted synchronous reluctance motor. In: 2019 IEEE Applied Power Electronics Conference and Exposition (APEC), pp. 1885–1890 (Mar 2019)
14. Luo, Y., Liu, C.: Elimination of harmonic currents using a reference voltage vector based-model predictive control for a six-phase PMSM motor. IEEE Trans. Power Electron. 34(7), 6960–6972 (2019)
15. Wang, T., et al.: Model predictive direct torque control of permanent magnet synchronous motors with extended set of voltage space vectors. IET Electr. Power Appl. 11(8), 1376–1382 (2017)
16. Zhu, W., Chen, C., Duan, S.: Model predictive control with improved discrete space vector modulation for three-level Vienna rectifier. IET Power Electron. 12(8), 1998–2004 (2019)
17. Xiong, C., et al.: A constant switching frequency multiple-vector-based model predictive current control of five-phase PMSM with non-sinusoidal back EMF. IEEE Trans. Ind. Electron. 67(3), 1695–1707 (2020)
18. Yang, X., et al.: Low-complexity model predictive control of AC/DC converter with constant switching frequency. IEEE Access. 8, 137 975–137 985 (2020)
19. Moon, H.-C., Lee, J.-S., Lee, K.-B.: A robust deadbeat finite set model predictive current control based on discrete space vector modulation for a grid-connected voltage source inverter. IEEE Trans. Energy Conv. 33(4), 1719–1728 (2018)
20. Wang, W., et al.: Model predictive torque control for dual three-phase PMSMS with simplified deadbeat solution and discrete space-vector modulation. IEEE Trans. Energy Conv. 1 (2021)
21. Hassine, I.M.-B., Naouar, M.W., Mrabet-Bellaaj, N.: Model predictive-sliding mode control for three-phase grid-connected converters. IEEE Trans. Ind. Electron. 64(2), 1341–1349 (Feb 2017)
22. Alam, K.S., et al.: Modified MPC with extended VVs for grid-connected rectifier. IET Power Electron. 11(12), 1926–1936 (2018)
23. Zhang, Y., Peng, Y., Qu, C.: Model predictive control and direct power control for PWM rectifiers with active power ripple minimisation. IEEE Trans. Ind. Appl. 52(6), 4909–4918 (Nov 2016)
24. Liu, X., Wang, D., Peng, Z.: A computationally efficient FCS-MPC method without weighting factors for NNPCs with optimal duty cycle control. IEEE ASME Trans. Mechatron. 23(5), 2503–2514 (2018)
25. Jin, T., et al.: A novel model predictive control via optimised vector selection method for common-mode voltage reduction of three-phase inverters. IEEE Access. 7, 95351–95363 (2019)
26. Shi, X., et al.: Low-complexity dual-vector-based predictive control of three-phase PWM rectifiers without duty-cycle optimization. IEEE Access. 8, 77049–77059 (2020)
27. Zhou, Z., et al.: Model predictive direct duty-cycle control for PMSM drive systems with variable control set. IEEE Trans. Ind. Electron. 68(4), 2976–2987 (2021)
28. IEEE Standards Coordinating Committee 21. IEEE standard for interconnection and interoperability of distributed energy resources with associated electric power systems interfaces, IEEE Std 1547-2018, pp. 1–138 (April 2018). (Revision of IEEE Std 1547-2003)
29. Jin, N., et al.: Finite states model predictive control for fault-tolerant operation of a three-phase bidirectional AC/DC converter under unbalanced grid voltages. IEEE Trans. Ind. Electron. 65(1), 819–829 (2018)
30. Ortega, R., et al.: Direct torque control of induction motors: stability analysis and performance improvement. IEEE Trans. Automat. Contr. 46(8), 1209–1222 (2001)
31. Chen, B.S., JoÓs, G.: Direct power control of active filters with averaged switching frequency regulation. IEEE Trans. Power Electron. 23(6), 2729–2737 (2008)

32. Escobar, G., et al.: Analysis and design of direct power control (DPC) for a three phase synchronous rectifier via output regulation subspaces. IEEE Trans. Power Electron. 18(3), 823–830 (2003)

33. Vazquez, S., et al.: A model-based direct power control for three-phase power converters. IEEE Trans. Ind. Electron. 55(4), 1647–1657 (2008)

34. Vekariya, A., et al.: Comparative study of lookup table approach of direct power control for three-phase DC/AC inverter. In: Dash, S.S. et al. (eds.), Artificial Intelligence and Evolutionary Computations in Engineering Systems, pp. 419–439. Springer Singapore (2017)